

Supplementary Data

A Multi-Center Randomized Proof-of-Concept Clinical Trial Applying [¹⁸F]FDG-PET for Evaluation of Metabolic Therapy with Rosiglitazone XR in Mild to Moderate Alzheimer's Disease

Sofia Tzimopoulou^a, Vincent J. Cunningham^a, Thomas E. Nichols^b, Graham Searle^a, Nick P. Bird^c, Prafull Mistry^c, Ian J. Dixon^c, William A. Hallett^a, Brandon Whitcher^a, Andrew P. Brown^a, Marina Zvartau-Hind^d, Narinder Lotay^d, Robert Y. K. Lai^e, Mary Castiglia^f, Barbara Jeter^f, Julian C. Matthews^g, Kewei Chen^{h,j,l}, Dan Bandy^{h,l}, Eric M. Reiman^{i,k,l}, Michael Gold^f, Eugeni A. Rabiner^{a,m} and Paul M. Matthews^{a,m,*}

^aGlaxoSmithKline Clinical Imaging Centre, Hammersmith Hospital, London, UK

^bDepartment of Statistics and Warwick Manufacturing Group, University of Warwick, Coventry, UK

^cGlaxoSmithKline Discovery Biometrics, Harlow, UK

^dGlaxoSmithKline Neurosciences Medicine Development Centre, London, UK

^eGlaxoSmithKline Neurosciences Discovery Medicine, Harlow, UK

^fGlaxoSmithKline Neurosciences Medicine Development Centre, Research Triangle Park, NC, USA

^gSchool of Cancer and Enabling Sciences, Wolfson Molecular Imaging Centre, University of Manchester, Manchester, UK

^hBanner Alzheimer's Institute and Positron Emission Tomography Centre, Banner Good Samaritan Medical Centre, Phoenix, AZ, USA

ⁱDepartment of Psychiatry, University of Arizona, Phoenix, AZ, USA

^jDepartment of Mathematics and Statistics, Arizona State University, Tempe, AZ, USA

^kNeurogenomics Division, Translational Genomics Research Institute, Phoenix, AZ, USA

^lArizona Alzheimer's Consortium, Phoenix, AZ, USA

^mDepartment of Clinical Neuroscience, Imperial College, London, UK

Accepted 27 August 2010

SUPPLEMENTARY INFORMATION

*Correspondence to: Professor P.M. Matthews, GSK Clinical Imaging Centre, Hammersmith Hospital, DuCane Road, London W12 0NN UK. Tel.: +44 208 008 6036; Fax: +44 208 008 6491; E-mail: paul.m.matthews@gsk.com.

This supplementary information describes further data acquisition, reconstruction, pre-processing, and methods of analysis.

IMAGING

PET Scanning

The dynamic PET scanning protocol consisted of 1×30 s, 1×10 s, 12×5 s, 2×10 s, 3×30 s, 3×60 s, 2×120 s and 10×300 s frames. The first 30 s blank frame was followed by a slow bolus injection of 170 MBq of FDG over 20 s. The PET scanners used included the Siemens HR+ , which was used for 52 subjects (University of Michigan, US [3 placebo, 3 RSG-XR], Banner Alzheimer's Institute, US [18 placebo, 19 RSG-XR], General Massachusetts Hospital, US [2 placebo, 4 RSG-XR], McGill University, Canada [2 placebo , 1 RSG-XR]), the GE Advance, used for 14 subjects (Duke University, US [7 placebo, 7 RSG-XR]), the Siemens ECAT HRRT, used for 7 subjects (University of Manchester, UK [4 placebo, 3 RSG-XR]), and the GE Discovery ST, used for 3 subjects (St Thomas Hospital, UK [2 placebo, 1 RSG-XR]). All of the subjects had their baseline and follow-up PET scans performed on the same scanners with the exception of one subject in the RSG-XR group that had a 12 month scan only on a GE Discovery STE (Duke University, US).

MRI scanning

The scanners used included the GE Genesis Signa 1.5 T, used for 63 subjects (University of Michigan, US [3 placebo, 3 RSG-XR], Duke University, US [7 placebo, 7 RSG-XR], Banner Alzheimer's Institute, US [18 placebo, 17 RSG-XR], McLean University, US [2 placebo, 4 RSG-XR], University of Arizona, US [0 placebo, 2 RSG-XR]), the Philips Intera 1.5 T, used for 7 subjects (University of Manchester, UK [4 placebo, 3 RSG-XR]), the Siemens Sonata Vision 1.5 T, used for 3 subjects McGill University, Canada [2 placebo, 1 RSG-XR]), the Siemens Magnetom Symphony 1.5 T, used for 2 subjects (The Wessex Nuffield Hospital, UK [2 placebo, 0 RSG-XR]), and the Siemens Symphony 1.5 T, used for 1 subject (Great Western Hospital, UK, [0 placebo, 1 RSG-XR]).

The GE scanner employed an SPGR sequence TE = 5.4 ms, Flip angle = 15 degrees, TI = 650 ms, NEX = 1, bandwidth 32 kHz, FOV = 240 mm, matrix = $256 \times 256 \times 124$, slice thickness = 1.5 mm. A 3D MPRAGE sequence was employed on Siemens scanners with the parameters TE = 3.44 ms, flip angle = 7 degrees, TI = 1000 ms, TR = 2730 ms, NEX = 1, bandwidth 190 Hz/pixel, FOV read 256 mm, matrix = $256 \times 256 \times 256$, Slices/ slab = 128 and slice thickness

= 1.33 mm. For the only Philips scanner a SPGR sequence was used; the scanning parameters were TE = 4 ms, Flip angle = 8.0 degrees, TI = 864.3 ms, NEX = 1, bandwidth approximately 180 Hz, FOV = 240 mm, matrix = $256 \times 256 \times 170$, slice thickness = 1.2 mm.

DATA PROCESSING AND ANALYSIS

Image reconstruction and pre-processing

Three-dimensional re-projection (3DRP) or Fourier re-binning (FORE), combined with two dimensional (2D) reconstruction or 3D ordinary Poisson ordered-subsets expectation maximization (OP-OSEM) were used for image reconstruction [1–3]. All sites were instructed to apply dead time correction, randoms correction, normalization, geometric correction, measured attenuation correction, scatter correction, axial and transaxial ramp filters. In contrast to the image pre-processing procedures subsequently developed in ADNI [4], this study did not smooth the images acquired on different imaging systems to a common spatial resolution.

Dynamic PET images were corrected for frame-wise subject head motion and registered to the corresponding MRI via rigid body registration, with normalized mutual information as cost function. The brain volume was extracted from the whole head MRI and segmented to generate a grey matter map. The MNI152 template [5] and corresponding anatomical human brain atlas [6] were nonlinearly warped onto each subject's MRI brain image. The warped atlas was then applied in conjunction with the grey matter map to the PET dynamic in order to generate time activity curves (TACs) for the grey matter in the regions of interest (ROIs). TACs were obtained for global grey matter and the following bilateral ROIs: posterior cingulate gyrus, parietal lobe, posterior temporal lobe, frontal lobe, cerebellum and medial temporal lobe (consisting of hippocampus, amygdala, medial anterior temporal lobe and parahippocampal ambiens gyrus). All rigid body image registrations, non-linear warps and MRI segmentation were performed using SPM5b [<http://www.fil.ion.ucl.ac.uk/spm>]. The brain extraction process was performed with FSL3.3.5 [<http://www.fmrib.ox.ac.uk/fsl>].

The results of brain image extraction and segmentation were quality checked by visual inspection. PET motion correction, PET-MRI co-registration, atlas warp to subject's MRI and subsequent PET alignment and grey mask images were also checked by visual inspec-

tion. Image quality control (QC) failures after blinded review included scans with unavailable scan and/or blood data in the measurement interval, scans with faults at FDG injection (infiltration) or PET acquisition and scans associated with incorrect blood data. Five subjects were excluded from the subsequent analysis due to unacceptable image or data quality at the baseline. Additional QC failures at individual timepoints of 1, 6, and 12 months included 1, 1 and 2 scans respectively.

Data supporting analysis based on principles of kinetic modeling

Fully quantitative estimation of CMR_{glu} from dynamic $[^{18}F]FDG$ -PET scans is based on a two tissue compartmental model with rate constants K_1 and k_2 describing the exchange of $[^{18}F]FDG$ between plasma and tissue across the blood-brain barrier, a rate constant, k_3 , describing the phosphorylation and ‘trapping’ of the tracer as $[^{18}F]FDG$ phosphate, and a rate constant, k_4 , often assumed to be negligible, which accounts for de-phosphorylation [7]. This model can be used to describe the characteristic accumulation of total radioactivity in brain during an FDG scan, with an early phase dominated by the exchange across the barrier followed by an approach to a near irreversible accumulation of the phosphate. Application of the model and estimation of the parameters requires an input function describing the time course of the concentration of $[^{18}F]FDG$ in arterial plasma throughout the PET following intravenous administration of the tracer or the image-derived input function [8,9]. The macroparameter of interest arising from this model is the combined forward rate constant (K_i) for $[^{18}F]FDG$ which is defined as

$$K_i = \frac{K_1 k_3}{k_2 + k_3}$$

This parameter may be obtained from the linear terminal slope of a Patlak plot [10,11]

$$\frac{c_t(t)}{c_p(t)} = K_i \frac{\int_0^t c_p(s) ds}{c_p(t)} + \alpha$$

where t is time, α is an effective volume of distribution, and $c_p(t)$ and $c_t(t)$ are the concentration time courses of $[^{18}F]FDG$ in plasma and tissue respectively. Alternatively K_i can be approximated by the simple PET quantifier known as the Fractional Uptake Rate (FUR) [12–14]:

$$FUR = \frac{c_t(t)}{\int_0^t c_p(s) ds} \approx K_i$$

under the assumption of negligible effective volume of distribution at late times after injection.

The cerebral metabolic rate for glucose then is given by:

$$CMR_{glu} = K_i \frac{c_p^{glu}}{LC}$$

where c_p^{glu} is the concentration of native glucose in plasma and LC (the so-called ‘‘lumped constant’’) accounts for the kinetic differences between native glucose and the deoxy analogue.

In the present study protocol it was not possible to obtain arterial blood samples on a routine basis. In order to take into account the delivery of $[^{18}F]FDG$ to the tissue and the concentration of native glucose in plasma without a direct measure of the arterial input function we therefore defined a pragmatic index of the combined forward rate constant as:

$$K_i^{index} = \frac{c_t^*}{c_p^* \times t}$$

where c_t^* is the average concentration of radioactivity in the tissue over the last 30 min of the 60 min scan calculated as the frame average TAC of the last 6 frames of the PET dynamic, c_p^* is the average plasma radioactivity calculated from the venous blood samples collected within the last 30 min of the scan and $t = 45$ min.

The K_i^{index} relates to FUR as:

$$K_i^{index} = FUR \text{ Ratio}$$

where $Ratio$ is defined as:

$$Ratio = \frac{\int_0^t c_p(s) ds}{c_p^* t}$$

We have hypothesized that if $Ratio$ can be considered constant across subjects for a specific time t then K_i^{index} will be linearly proportional to FUR and subsequently to K_i . The hypothesis is true if the shape of the input function is the same across subjects and timepoints.

Data collected from another study using a similar patient population under a scanning protocol identical except that it allowed inclusion of arterial data collection (GSK Protocol: AVA100930, clinical trials identifier: NCT00334568, number of PET scans analyzed: 10) confirmed a good correlation of K_i^{index} to the true K_i : $K_i = 0.644 K_i^{index} - 4.1722$, gradient confidence

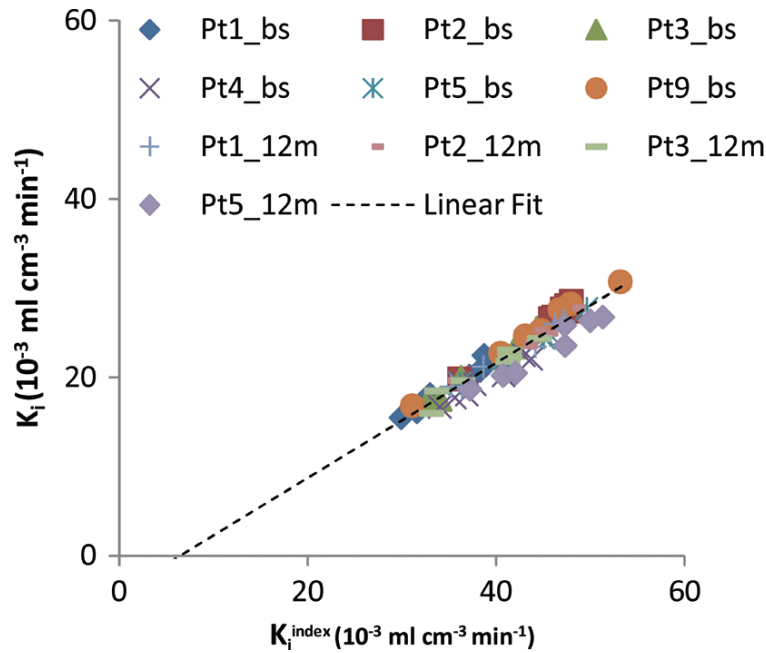


Fig. S1. Correlation of K_i to K_i^{index} . Data shown include results from individual ROIs and global grey matter from 6 baseline and 4 twelve month scans (active: Pt2_12m, Pt3_12m, Pt5_12m, placebo Pt1_12m), Pt=patient, bs=baseline, 12m=12 months.

interval (0.598, 0.691), intercept confidence interval ($-6.120, -2.224$), $R^2 = 0.9153$ (Fig. S1). Similar offset (mean, CI: $-3.973, (-5.336, -2.610)$) was observed when K_i was regressed on FUR (graph not shown). The negative offset is expected due to the non zero effective volume of distribution in the Patlak equation and is not of primary concern on assessments of longitudinal differences. The area $\int_0^t c_p(s)ds$ correlated well with the area c_p^*t (Fig. S2): gradient confidence interval (1.494, 1.969) intercept confidence interval ($-3.686, 94.378$), $R^2 = 0.9622$, supporting the assumption of $Ratio$ being approximately constant.

Use of this index makes the same assumptions as autoradiographic methods for which it is assumed that there is a linear relationship between analogue phosphorylation rate and the concentration of radioactivity in the tissue at late times [15,16]. Other already validated assumptions in the literature include a proportionality between the concentration of radioactivity in late venous samples and the integral of the arterial input function [17] as well as negligible effective volume of distribution for late scan time points in the Patlak equation [14]. K_i^{index} is intended to describe an analogous trend of the true metabolic rate of FDG. Under the validity of the approximation that the shape of the FDG input function is the same across study subjects

and timepoints K_i^{index} forms a quantitative measure of K_i and allows for assessment of global changes.

A corresponding index for the metabolic rate for glucose was then calculated by:

$$CMR_{glu}^{index} = K_i^{index} c_p^{glu}$$

assuming no changes in the Lumped Constant.

With these formulations, possible drug effects arising from changes in systemic plasma glucose concentration (reflected in c_p^{glu} changes) can be considered in addition to those arising from increased transport or phosphorylation of FDG (K_i^{index} changes).

Thus this approach is based on kinetic analysis principles widely used for quantitative analysis of brain CMR_{glu} [7,10,11] and distinguishes between FDG uptake and native glucose uptake.

Further data regarding the analysis based on an empirically pre-defined statistical region-of-interest derived from the ADNI

The empirically pre-defined “spared” ROI includes 2,454 voxels from white matter and cerebellar regions known to be relatively spared neuropathological change in subjects with mild AD. The “statistical” ROI (sROI), which includes 32,807 voxels, resembles the pattern of regional 12-month decline in [^{18}F]FDG uptake de-

Table 1

Adjusted 12 month mean change from baseline in global grey matter for CMR_{glu}^{index} ($\mu\text{g cm}^{-3} \text{ min}^{-1}$) or the CMR_{ratio} (a unitless ratio) with CI(95%) and p-values (uncorrected), for the subgroup of patients of E3/3 and E3/4 genotype. Percentage change from baseline is given in parentheses. Abbreviations: CI, confidence interval; RSG, rosiglitazone

Genotype	Index	RSG-XR	Placebo	Difference (RSG-XR-Placebo)	Difference CI(95%)	Difference p-value
E3/3	CMR_{glu}^{index}	-1.607 (-3.6%)	-4.413 (-10.0%)	2.807 (6.4%)	(-7.767, 13.380)	0.60
	CMR_{ratio}	-0.0691 (-6.2%)	-0.0192 (-1.7%)	-0.0499 (-4.5%)	(-0.0935, -0.0063)	0.03
E3/4	CMR_{glu}^{index}	-5.842 (-13.2%)	-5.742 (-13.0%)	-0.100 (-0.2%)	(-8.627, 8.427)	0.98
	CMR_{ratio}	-0.0378 (-3.4%)	-0.0709(-6.3%)	0.0330 (2.9%)	(-0.0027, 0.0688)	0.07

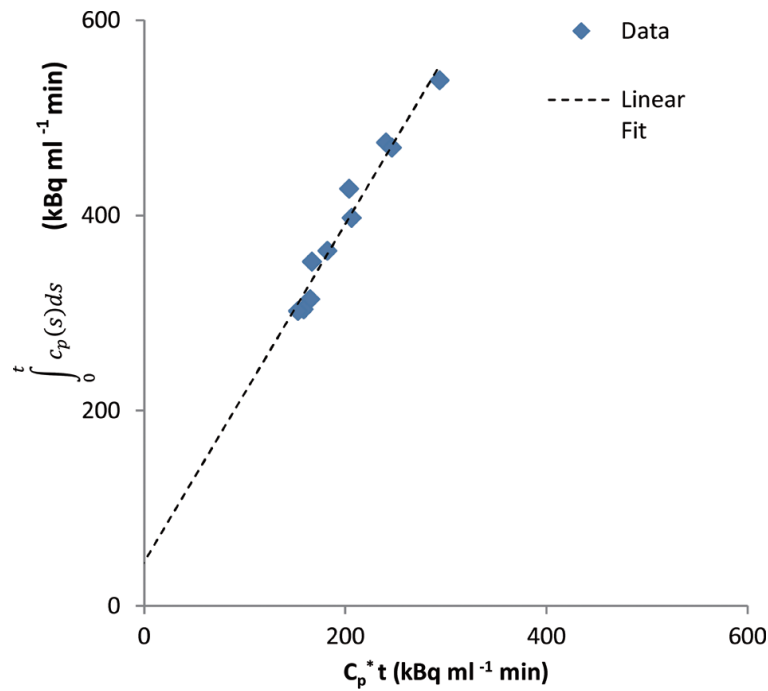


Fig. S2. The area under the arterial input function ($\int_0^t c_p(s)ds$) is highly correlated to its simpler approximation c_p^*t used in the K_i^{index} with intercept value 0 included in the confidence interval, thus supporting the use of K_i^{index} as a PET quantifier. Data shown include results from 6 baseline and 4 twelve month scans (active: 3, placebo 1), individual *Ratio* values: 1.833, 1.904, 1.905, 1.915, 1.926, 1.974, 1.976, 1.998, 2.097, and 2.114.

finned using Statistical Parametric Mapping (SPM) and includes voxels in posterior cingulate, medial and lateral parietal, medial and lateral temporal, frontal and occipital cortices bilaterally.

APOE genotype analysis according to specific genotype

Subject numbers allowed post hoc analysis to test for possible drug effect on genotypes E3/3 (3 placebo, 10 RSG-XR), E3/4 (11 placebo, 5 RSG-XR). This analysis aimed to unmask any possible drug effect covered by the inclusion of multiple genotypes in the APOE4 positive and negative populations. The results (Table S1)

agree with the trends observed in the general APOE4 populations namely a non significant smaller metabolic decrease in the APOE4 negative active group in primary analysis in contrast to a non significant smaller decrease observed in the APOE4 positive group in secondary analysis. The difference in results indicate limited statistical power due to small and imbalance sample sizes and confirm the lack of a drug effect.

ACKNOWLEDGMENTS

The authors would like to thank the principal investigator of GSK study AVA100930 John Hodges

(MRC Cognition and Brain Sciences Unit, Addenbrookes Hospital, Cambridge, UK), Dr Timothy Fryer and all staff involved in the study scans for leading in acquisition of data used to support this qualification.

References

- [1] Defrise M, Kinahan PE, Townsend DW, Michel C, Sibomana M, Newport DF (1997) Exact and approximate rebinning algorithms for 3-D PET data. *IEEE Trans Med Imaging* **16**, 145-158.
- [2] Hudson HM, Larkin RS (1994) Accelerated image reconstruction using ordered subsets of projection data. *IEEE Trans Med Imaging* **13**, 601-609.
- [3] Kinahan PE, Rogers JG (1989) Analytic three-dimensional image reconstruction using all detected events. *IEEE Trans Nucl Sci* **36**, 964-968.
- [4] Chen K, Langbaum JBS, Fleisher AS, Reschke BS, Lee W, Xiaofen L, Napatkamon A, Bandy D, Alexander GE, Thompson PM, Foster NL, Harvey DJ, de Leon MJ, Koeppe RA, Jagust WJ, Weiner MW, Reiman EM (2010) Twelve month metabolic declines in probable Alzheimer's disease and amnesic mild cognitive impairment assessed using an empirically pre-defined statistical region-of-interest: findings from the Alzheimer's disease neuroimaging initiative. *Neuroimage* **51**, 654-664.
- [5] Mazziotta J, Toga A, Evans A, Fox P, Lancaster J, Zilles K, Woods R, Paus T, Simpson G, Pike B, Holmes C, Collins L, Thompson P, MacDonald D, Iacoboni M, Schormann T, Amunts K, Palomero-Gallagher N, Geyer S, Parsons L, Narr K, Kabani N, Le Goualher G, Boomsma D, Cannon T, Kawashima R, Mazoyer B (2001) A probabilistic atlas and reference system for the human brain: International Consortium for Brain Mapping (ICBM). *Philos Trans R Soc Lond B Biol Sci* **356**, 1293-1322.
- [6] Hammers A, Allom R, Koeppe MJ, Free SL, Myers R, Lemieux L, Mitchell TN, Brooks DJ, Duncan JS (2003) Three-dimensional maximum probability atlas of the human brain, with particular reference to the temporal lobe. *Hum Brain Mapp* **19**, 224-247.
- [7] Phelps ME, Huang SC, Hoffman EJ, Selin CJ, Sokoloff L, Kulh DE (1979) Tomographic measurement of local cerebral glucose metabolic rate in humans with [¹⁸F]2-fluoro-2-deoxy-D-glucose: Validation of method. *Ann Neurol* **6**, 371-388.
- [8] Chen K, Bandy D, Reiman E, Huang SC, Lawson M, Feng D, Yun LS, Palant A (1998) Noninvasive quantification of the cerebral metabolic rate for glucose using positron emission tomography, ¹⁸F-fluoro-2-deoxyglucose, the Patlak method, and an image-derived input function. *J Cereb Blood Flow Metab* **18**, 716-723.
- [9] Chen K, Chen X, Renaut R, Alexander GE, Bandy D, Guo H, Reiman EM (2007) Characterization of the image-derived carotid artery input function using independent component analysis for the quantitation of [¹⁸F] fluorodeoxyglucose positron emission tomography images. *Phys Med Biol* **52**, 7055-7071.
- [10] Patlak CS, Blasberg RG, Fenstermacher JD (1983) Graphical evaluation of blood-to-brain transfer constants from multiple-time uptake data. *J Cereb Blood Flow Metab* **3**, 1-7.
- [11] Patlak CS, Blasberg RG (1985) Graphical evaluation of blood-to-brain transfer constants from multiple-time uptake data. Generalizations. *J Cereb Blood Flow Metab* **5**, 584-590.
- [12] Ishizu K, Yonekura Y (1995) Clarification of a fractional uptake concept-Reply, p. 712.
- [13] Ishizu K, Nishizawa S, Yonekura Y, Sadato N, Magata Y, Tamaki N, Tsuchida T, Okazawa H, Miyatake S, Ishikawa M, Kikuchi H, Konishi J (1994) Effects of hyperglycemia on FDG uptake in human brain and glioma. *J Nucl Med* **35**, 1104-1109.
- [14] Thie M (1995) Clarification of a fractional uptake concept. *J Nucl Med* **36**, 711-712.
- [15] Hutchins GD, Holden JE, Koeppe RA, Halama JR, Gately SJ, Nickles RJ (1984) Alternative approach to single-scan estimation of cerebral glucose metabolic rate using glucose analogs, with particular application to ischemia. *J Cereb Blood Flow Metab* **4**, 35-40.
- [16] Rhodes CG, Wise RJ, Gibbs JM, Frackowiak RS, Hatazawa J, Palmer AJ, Thomas DG, Jones T (1983) In vivo disturbance of the oxidative metabolism of glucose in human cerebral gliomas. *Ann Neurol* **14**, 614-626.
- [17] Takagi S, Takahashi W, Shinohara Y, Yasuda S, Ide M, Shohtsu A, Seio T (2004) Quantitative PET cerebral glucose metabolism estimates using a single non-arterialized venous-blood sample. *Ann Nucl Med* **18**, 297-302.